ACS APPLIED MATERIALS & INTERFACES

Letter

www.acsami.org

Low-Temperature Sputtered Nickel Oxide Compact Thin Film as Effective Electron Blocking Layer for Mesoscopic NiO/$CH_3NH_3PbI_3$ Perovskite Heterojunction Solar Cells

Kuo-Chin Wang,[†] Po-Shen Shen,[†] Ming-Hsien Li,[†] Shi Chen,[†] Ming-Wei Lin,[‡] Peter Chen,*[,†,§,∥] and Tzung-Fang Guo[†,§,∥]

[†]Department of Photonics, [§]Research Center for Energy Technology and Strategy (RCETS), and [∥]Advanced Optoelectronic Technology Center (AOTC), National Cheng Kung University, Tainan, Taiwan 701

[‡]National Synchrotron Radiation Research Center (NSRRC), 101 Hsin-Ann Road, Hsinchu Science Park, Hsinchu, Taiwan

Supporting Information

ABSTRACT: We introduce the use of low temperature sputtered NiOx thin film, which substitutes the PEDOT−PSS and solution-processed NiOx as an effective electron blocking layer for mesoscopic NiO/$CH_3NH_3PbI_3$ perovskite solar cells. The influences of film thickness and oxygen doping on the photovoltaic performances are scrutinized. The cell efficiency has been improved from 9.5[1] to 10.7% for devices using NiOx fabricated under pure argon atmosphere. With adequate doping under 10% oxygen flow ratio, we achieved power conversion efficiency of 11.6%. The procedure is large area scalable and has the advantage for cost-effective perovskite-based photovoltaics.

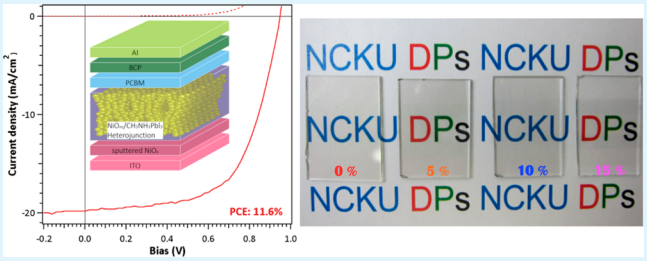

KEYWORDS: *pervoskite solar cell, sputtering, NiOx thin film, mesoscopic heterojunction, low temperature process*

Organic−inorganic hybrid metal halide perovskite materials have received intensive attentions since their breakthrough after the successes in solid heterojunction devices in 2012.[2,3] The rapid progresses of this research field over the past few years have remarkably advanced the conversion efficiencies over 15%.[4−6] Perovskite-based solar cell is considered as a promising emerging technology due to their characteristics of cost-effective solution process, high power conversion efficiency (PCE) and superior photonic properties in terms of light absorption and carrier transport.

Various device configurations have been proposed and demonstrated with high PCE. Dye-sensitized solar cells (DSCs) like mesoscopic devices were initially the structure employed which the perovskite material served as a light harvester.[2,4,7] Planar heterojunction (PHJ) thin film architectures,[5,6,8−10] on the other hand, sandwiched the perovskite between effective charge selective contact materials to accomplish the photovoltaic action. Among the PHJ devices, a typical structure is composed of materials similar to organic photovoltaics like poly(3,4-ethyl- enedioxythiophene) poly-(styrene-sulfonate) (PEDOT:PSS) and [6,6]-phenyl C61-butyric acid methyl ester (PCBM) where the perovskite material is inserted as absorber and electron donor. This type of OPV-like thin film perovskite solar cells using a low-temperature process has achieved 11.5%.[11] However, the experiences from OPV research have shown concerns of PEDOT:PSS for long-term stability.[12,13] Providing more stable constituents for perovskite-based photovoltaics remained a challenge as most efficient charge separation junctions with perovskite required organic materials. In our previous report, we have replaced the PEDOT:PSS with solution processed NiOx electrode interlayer for hole extraction.[14] Furthermore, we have introduced the mesoscopic NiO layer into this OPV-like structure to host the perovskite material in order to improve light harvesting efficiency (LHE) and morphology control.[1] Recently, several groups have successfully reported this p-type sensitized NiO/perovskite heterojunction solar cell.[15,16] The elimination of the organic hole transporter (or hole collecting layer) shall improve the device stability and provide versatile choices for materials selection and device design. Other inorganic materials such as CuI and CuSCN have been shown to be a potential candidate for this purpose.[17−19]

Metal oxide p-type semiconductors are alternative hole transport materials for pereovskite-based solar cells owing to their transparency in the visible region, good chemical stability and various selections in terms of the VB energy level. For the organic bulk heterojunction (BHJ) solar cells, p-type metal oxide semiconductors including NiO,[20] V_2O_5,[21] and MoO_3[13,22] have been utilized as hole extraction layer. In dye-sensitized solar cells (DSCs), many metal oxides such as NiO, Cu-based delafossite ($CuMO_2$, M = Al, Ga, or Cr), have been applied as electrode for p-type sensitization.[23,24] Recently, NiO/perovskite

Received: June 7, 2014
Accepted: July 23, 2014
Published: July 23, 2014

heterojunction solar cells have been successfully demonstrated with decent efficiencies.[1,15,16] In this article, we developed a low-temperature sputtered NiOx thin film as a functional hole extraction and electron blocking layer for the organic and inorganic hybrid perovskite-based solar cells. The efficiencies are greatly enhanced and the device reproducibility is significantly improved compared with the devices fabricated by solution-processed NiOx thin film. We studied the effects of film thickness and doping ratio of oxygen flow during the low-temperature sputtered NiOx on the photovoltaic performances of mesoscopic NiO/$CH_3NH_3PbI_3$ heterojunction solar cells. The characterization of material properties of sputtered NiOx thin film was carried out by X-ray diffraction (XRD) and Mott–Schottky analysis. Optical property of sputtered NiOx compact layer was characterized by UV–visible spectroscopy. Scanning electron microscope (SEM) was conducted to examine the morphology of NiOx thin film. X-ray photoelectron spectroscopy (XPS) was performed to characterize the surface chemical environment.

The device architecture is illustrated in Scheme 1. The details of the experimental methods are described in the Supporting Information. The process variables for RF sputtering deposition conditions of NiOx compact layer were summarized in Table 1. The main deposition parameters investigated are oxygen flow ratios and sputtering time. Samples of series A were fabricated by different deposition time under pure Ar as working gas without oxygen doping, and those of series B were prepared under reactive atmosphere with various oxygen flow ratios performed with the same deposition time of 150 s. The devices using the corresponding NiOx sputter film will be denoted as the notations listed in Table 1 through the whole article.

Scheme 1. Device Structure of NiO/Perovskite Heterojunction Solar Cells

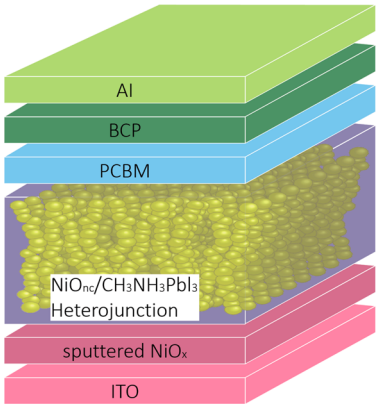

Table 1. Notation List of NiOx Compact Layer Prepared under Various Sputtering Parameters (oxygen flow ratio and sputtering time)

notation of film[a]	oxygen flow ratio (O_2/Ar+O_2) (%)				sputtering time (s)					
	0	5	10	15	0	100	125	150	175	200
A-0-0	○				♦					
A-0-100	○					♦				
A-0-125	○						♦			
A-0-150	○							♦		
A-0-175	○								♦	
A-0-200	○									♦
B-5-150		○						♦		
B-10-150			○					♦		
B-15-150				○				♦		

[a]A denotes the sample fabricated with pure Ar working gas, whereas B presents the samples deposited with reactive mixture of Ar+O_2. The second digit describes the oxygen flow ratio (O_2/Ar+O_2). The third digit displays the deposition time.

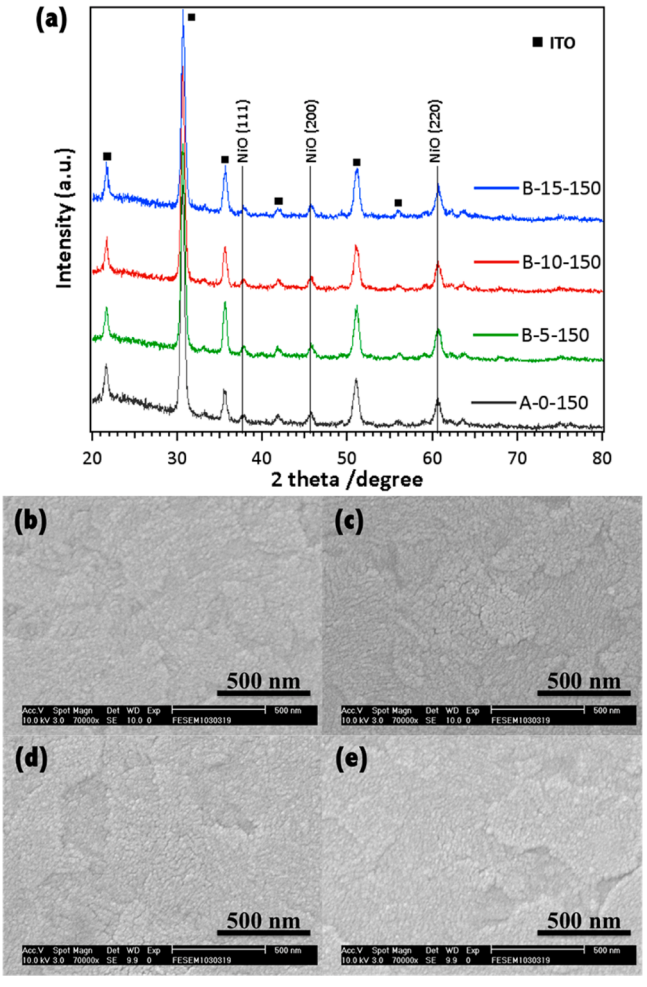

Figure 1. (a) X-ray diffraction patterns of sputtered NiOx films doped with various oxygen flow ratios. The square markers represent the XRD peaks of ITO conductive layer. Top view SEM images of NiOx thin film doped with (b) 0, (c) 5, (d) 10, and (e) 15% of oxygen flow ratio. The magnification of all SEM images is 70 000 with the scale bar of 500 nm.

The X-ray diffraction patterns for A-0-150, B-5-150, B-10-150, and B-15-150 are displayed in Figure 1a. The XRD patterns are assigned to the three main NiO peaks which refer to planes (111), (200), and (220), respectively. The XRD results confirm the existence of NiOx thin film deposited on ITO-coated substrate. On the other hand, it is observed that plane (220) of B-15–150 is slightly broader than that of the others. This is probably due to the interstitial oxygen defects that being introduced by the excess doping from high oxygen/Ar flow ratio during sputtering deposition.[25] Figure 1b–e showed top views of SEM images of NiOx films prepared by various oxygen flow ratios. The grain size of all NiOx films is fairly small (<100 nm), and the surface is closely packed with

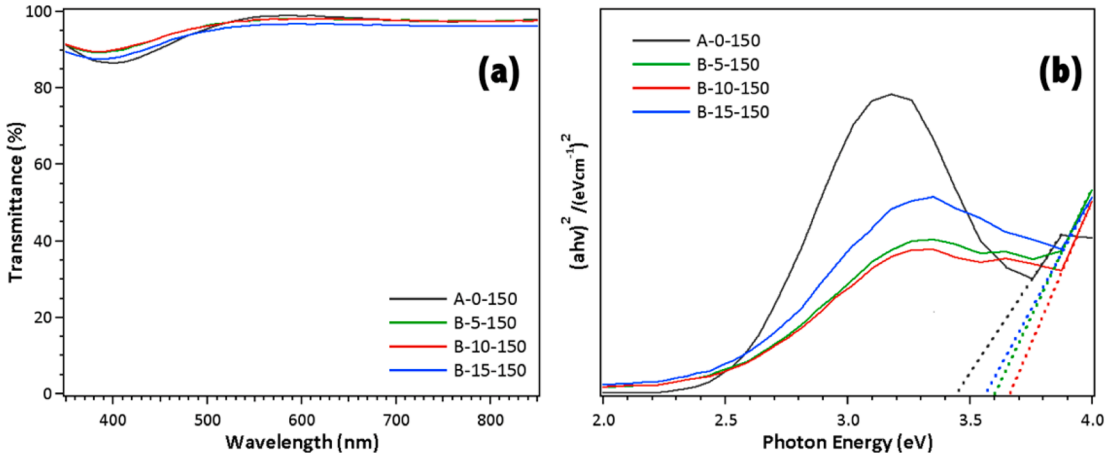

Figure 2. (a) Optical transmittance spectra of sputtered NiOx films prepared using various oxygen flow ratios. (b) Optical energy band gap of NiOx films fabricated with different oxygen flow ratios.

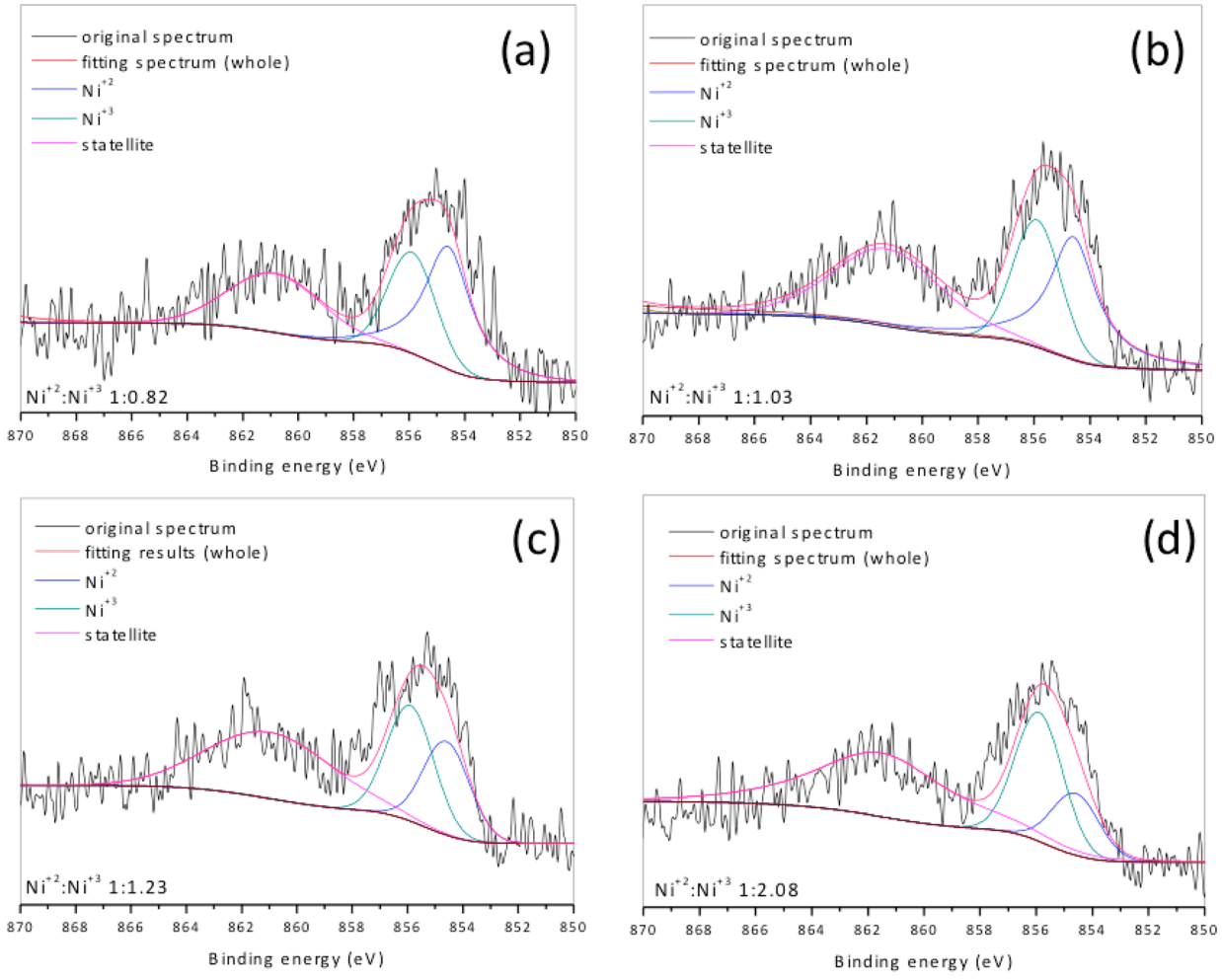

Figure 3. X-ray photoelectron spectroscopy analysis with deconvolution of Ni^{2+} and Ni^{3+} of Ni $2p_{3/2}$ spectra of NiOx thin film doped with (a) 0, (b) 5, (c) 10, and (d) 15% of oxygen flow ratio.

NiOx thin film. Mott−Schottky plots measured from electrochemical impedance spectroscopy showed negative slopes of $1/C_{sc}^2$ vs applied potential indicating that the sputtered NiOx thin films behaved as p-type semiconductors (see Figure S1 in the Supporting Information).

Figure 2a presents the optical transmittance spectra of NiOx thin films for sample A-0-150, B-5-150, B-10-150, and B-15-150. The variations of transmission are very marginal for such a thin layer with thickness around 10 nm and the interference could have influences on the spectra. The photos of sputtered NiOx films doped with various oxygen flow ratios on ITO substrates are illustrated in Figure S2 in the Supporting Information. The optical absorption coefficient (α) can be estimated from three items, consisting of the film thickness (t),

the optical transmittance (T) and reflectance (R), using eq 1. The absorption coefficient (α) obeys the following relationship of incident photon energy with the band gap using eq 2.

$$\alpha = -\frac{1}{t}\left[\ln\frac{T}{(1-R^2)}\right] \quad (1)$$

$$(\alpha h\nu) = (h\nu - E_g)^n \quad (2)$$

E_g means the separation between the bottom of the conduction band (CB) and the top of the valence band (VB), and $h\nu$ is the incident photon energy with n as a constant. The value of n equals to 2 or 1/2 corresponding to the absorption behavior for direct and indirect optical transition, respectively. The plot of $(\alpha h\nu)^2$ as a function of photon energy of NiOx films fabricated under various oxygen flow ratios is presented in Figure 2b. As Figure 2b shows, the optical energy band gap of films increases from 3.43 to 3.65 eV with the oxygen flow ratio rising from 0 to 10%. While increasing doping ratio to 15%, the band gap of the film decreases to 3.56 eV. This trend on the changes of energy band gap has good correlations with the flat band potential obtained from Mott−Schottky plots (see Figure S1 in the Supporting Information) where the oxygen-doped films (B-5-150, B-10-150) have more positively shifted flat band positions except for sample B-15-150. Those values of the band gap are in agreement with the energy band gap reported in the literature.[26] In general, optical transitions in metal oxide are associated with various energy states within the material. The major transition is related to the near band edge (NBE) between CB and VB, whereas the other transitions corresponds to the energy states introduced by the intraband defects such as metal deficiency or oxygen excess for p-type metal oxide semiconductor. The film fabricated under the highest oxygen flow ratio (B-15-150) resulted in a reduced band gap is ascribed to the nonstoichiometry defects of Ni vacancy (V''_{Ni}) or interstitial oxygen. The Ni vacancies and Ni^{3+} energy states in NiOx material are located above the top of VB that would receive electrons from VB and act as a p-type doping. Because nickel oxide is a well-known metal deficient p-type semiconductor, under excess oxygen atmosphere, it is likely that the defects are gradually formed as the following equation[27]

$$2Ni^{+2} + \frac{1}{2}O_2(g) \rightarrow O^{2-} + V^0_{Ni} + 2Ni^{+3} \quad (3)$$

where V^0_{Ni} stands Ni vacancy which could further forms singly (V'_{Ni}) or doubly (V''_{Ni}) ionized defects associated with hole generation ($V^0_{Ni} \rightarrow V'_{Ni} + h^+$ and $V'_{Ni} \rightarrow V''_{Ni} + h^+$). It was reported that interstitial oxygen defects or V''_{Ni} are native-acceptor-like defects. Furthermore, Ni^{3+} is also an acceptor for electron. Especially, V''_{Ni} is the most stable defect within band gap due to lower formation energy.[28] As can be seen in Figure 2b, there is one obvious peak observed between 3 and 3.5 eV, which suggested the formation of intraband energy states introduced by Ni vacancies or interstitial oxygen. To analyze the defect chemistry of the sputtered NiOx thin film, the chemical environments of NiOx thin films with various doping level are characterized by X-ray photoelectron spectroscopy (XPS). As shown in Figure 3, XPS spectrum corresponds to Ni $2p_{3/2}$ is located at 856 eV. The Ni^{2+} and Ni^{3+} are chosen to deconvolute the peak of Ni $2p_{3/2}$. The binding energy of the Ni^{2+} and Ni^{3+} of NiO and Ni_2O_3 are assigned to around 854 and 857 eV, respectively. As eq 3 shown, the Ni^{3+} are produced through Ni^{2+} to remain the electrical neutrality in the crystal. As a result, the number of the Ni^{3+} ions gradually increases with the oxygen doping concentration. From Figure 3a−d, the integrated peak area ratio of Ni^{3+}/Ni^{2+} is evaluated to be 0.82, 1.03, 1.23, and 2.08 as oxygen doping concentration increases from 0, 5, 10, to 15%, respectively. The results implied that the oxygen flow ratio has significant influences on the p-type characteristics and doping concentrations.

Previous literature has concluded that there is a dependence of photovoltaic performance on mesoporous film thickness due to the limit of charge (hole) diffusion length and recombination.[4] Therefore, we varied the mesoscopic NiO layer thickness by changing spin-coating rotational speed during deposition and applied the condition of 150 s deposition time to prepare sputtered NiOx compact layer. The photovoltaic parameters were presented in Table 2 and the $J-V$ curves of these devices

Table 2. Summary of Photovoltaic Parameters for Devices Fabricated with Different Mesoporous $NiO_{(nc)}$ Layer Thickness by Changing Spin-Coating Rotational Speed

	3000 rpm	4000 rpm	5000 rpm
V_{OC} (V)	0.90	1.00	0.92
J_{SC} (mA/cm^2)	17.75	17.4	16.91
FF	0.56	0.61	0.57
PCE (%)	8.89	10.7	9.00

are shown in Figure 4a. As we observed in Table 2, V_{OC} and J_{SC} obviously increase with 0.08 V and 0.5 mA cm^{-2} when rotational speed slows down from 5000 to 4000 rpm (film thickness of about 200 to 250 nm). The enhancements in V_{OC} and J_{SC} could be fairly attributed to the loading of perovskite light absorber resulting from increased mesoporous NiO layer (with film thickness of 320 nm), delivering the best cell efficiency of 10.7%. With further slowing rotational speed down to 3000 rpm, the V_{OC} and fill factor of device declined on the contrary. Apparently, further increasing film thickness led to higher charge (hole) transport resistance and more recombination, which caused a loss in V_{OC} and lower fill factor. According to the results, we apply 4000 rpm as the best spin-coating condition for mesoporous NiO layer preparation in the following discussion. The color of the resulting films showed significant visible range light harvesting. Its absorbance is shown in Figure S3 in the Supporting Information. The optical properties are similar to our previous results where both the absorption spectra and photo image of perovskite film coated on mesoscopic NiO are available.[1] A slightly reduced absorption between 500 and 750 nm due to film thickness limitation is reflected in the LHE value, which decreased from 90 to 70% (Figure 3c in reference1). This unsaturated light harvesting leads to the lower IPCE response in the corresponding absorption range.[15]

It is well-known that the thickness of TiO_2 compact layer has significant impact on the solid-state DSCs.[29] We expected the thickness of NiOx compact layer would have similar influences on the collection of photocurrent or the electron blocking effect. Consequently, the film thickness was controlled by varying the sputtering time from 100 to 200 s so as to explore the effect of thickness dependence of NiOx compact layer on the photovoltaic performance of mesoscopic NiO/$CH_3NH_3PbI_3$ heterojunction solar cells (Figure 4b). Because the deposited blocking NiOx films are extremely thin within few nanometer ranges, the thicknesses are estimated by

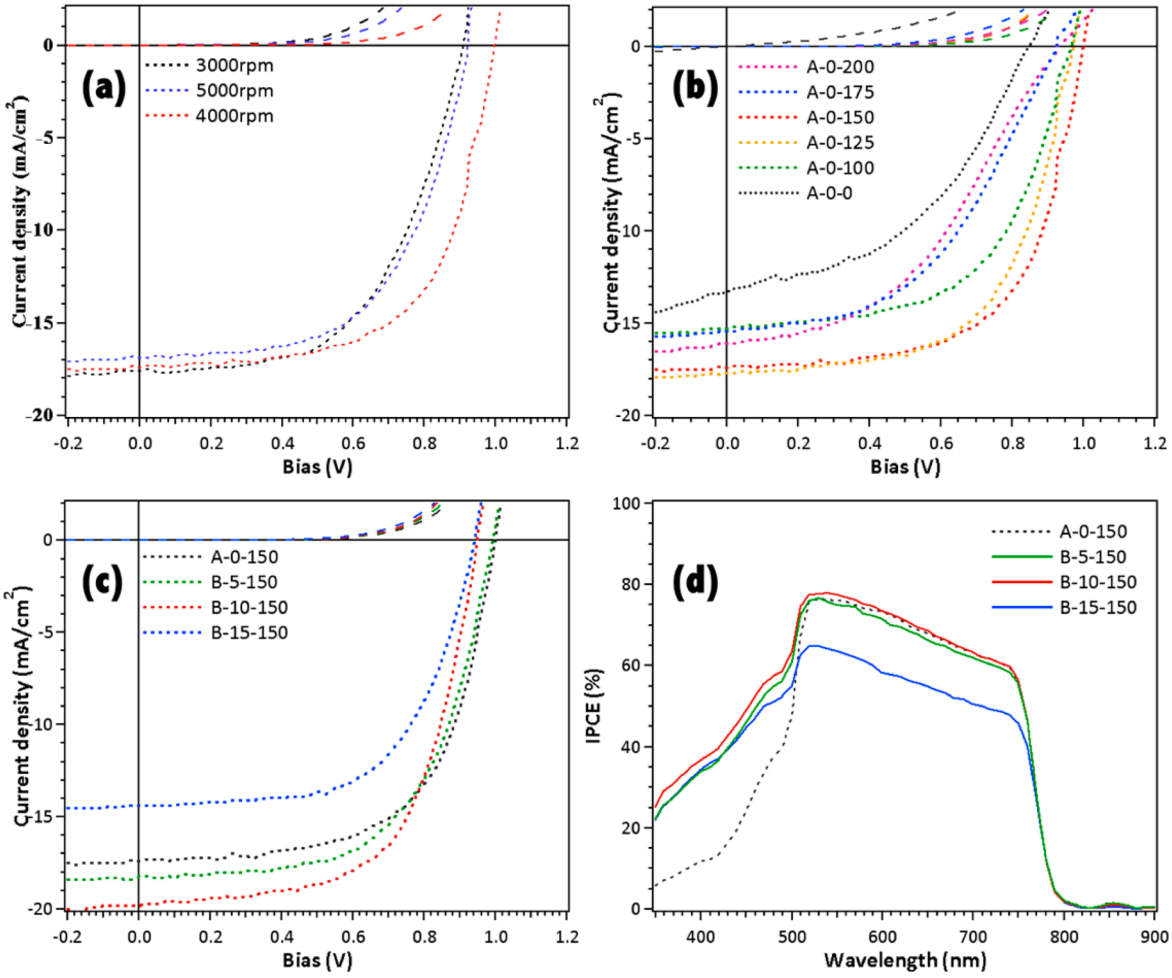

Figure 4. J–V characteristics measured under AM 1.5G solar irradiance (100 mW cm^{-2}) and dark for devices fabricated with (a) different mesoporous NiO layer thickness, and using NiOx films with (b) different deposition time and (c) different oxygen flow ratios. (d) IPCE curves for devices fabricated under various oxygen flow ratios in c.

Table 3. Summary of Photovoltaic Parameters for Devices Using NiOx Compact Layer Fabricated with Different Thickness without Oxygen Flow during Sputtering

	A-0-0	A-0-100	A-0-125	A-0-150	A-0-175	A-0-200
estimated NiOx thickness (nm)		6.0 ± 0.5	8.0 ± 0.5	10.0 ± 0.5	12.0 ± 0.5	14.0 ± 0.5
V_{OC} (V)	0.84	0.96	0.96	1.00	0.92	0.94
J_{SC}(mA/cm^2)	13.3	15.25	17.72	17.4	15.4	16.1
FF	0.45	0.57	0.598	0.61	0.48	0.43
PCE (%)	5	8.44	10.2	10.7	6.8	6.4

interpolation of film thickness deposited from a much longer time as shown in Table 3. Meanwhile, we also fabricated devices (A-0-0) without the NiOx compact layer. The photovoltaic parameters of devices made with different NiOx compact layer thickness without oxygen doping were summarized in Table 3. It is worth noting that, surprisingly, the device even without the NiOx compact layer (A-0-0) still performed photovoltaic action with 5% efficiency. However, this cell (device A-0-0) exhibited the lowest power conversion efficiency mainly due to much lowered voltage and fill factor compared with the other devices incorporating sputtered compact NiOx thin film. The addition of the NiOx compact layer significantly enhanced the rectifying current–voltage characteristic compared to that without compact layer. The usage of NiOx thin film is advantageous in providing electron-blocking effect and reduces charge recombination at interface between the holes in the ITO and the electrons in the photoactive perovskite layer. As a result, when the sputtering time raises from 100 to 150 s, the enhancement in short-circuit current density and power conversion efficiency is significant with the open-circuit voltage reaching as high as 1 V. However, we observed the devices with thicker compact layer (A-0-175 and A-0-200) delivered lower values of current density and fill factor (FF), leading to lower conversion efficiencies. It is clear that the device made of A-0-200 NiOx film suffered from the low fill factor of 0.43 which tremendously impaired the photovoltaic performance to an overall efficiency of 6.4%. This suggests that thick NiOx film would increase series resistance and prevent effective holes collection, causing a loss in photocurrent and deteriorated fill factor. Thus, the results

obviously implied that the thickness of NiOx compact layer plays a vital role in carrier extraction and electron blocking as interlayer between charge (hole) collective electrode (ITO) and active layer (perovskite). For the best condition of sputtering time with 150 s, the device A-0-150 delivered conversion efficiency of 10.7%, with open-circuit voltage of 1 V, short-circuit current density of 17.4 mA cm^{-2}, and fill factor of 0.61.

Several reports have investigated the effect of oxygen flow ratios on the electrical and optical properties of NiOx films fabricated by magnetron sputtering.[25,26,30] Thus, we present how sputtered NiOx compact layers prepared under different oxygen flow ratios affect the photovoltaic performances (Figure 4c). On the basis of the investigation of film thickness effect, we apply the condition of 150 s deposition time to examine the influences of oxygen doping on device performances. Devices B-5-150, B-10-150, and B-15-150 were fabricated to compare with device A-0-150 so as to explore the effect of oxygen doping during sputtering on the photovoltaic performance. Table 4 summarizes the photovoltaic characteristics of devices

Table 4. Summary of Photovoltaic Parameters for Devices Using NiOx Compact Layer Fabricated under Different Oxygen Flow Ratios

	A-0-150	B-5-150	B-10-150	B-15-150
V_{OC} (V)	1.00	1.00	0.96	0.94
J_{SC} (mA/cm^2)	17.4	18.2	19.8	14.4
FF	0.61	0.59	0.61	0.60
PCE (%)	10.7	10.8	11.6	8.1
integrated IPCE current (mA/cm^2)	14.06	15.15	15.63	12.99

for A-0-150, B-5-150, B-10-150, and B-15-150. Current–voltage characteristic curves of these devices are displayed in Figure 4c. We observed that device B-10-150 produced short-circuit current density as high as 19.8 mA cm^{-2}, which is improved by almost 20% than that of device A-0-150. As we have discussed in the transmittance spectra, the addition of oxygen flow resulted in very marginal changes in optical properties. We believe the phenomenal enhancement is a consequence of electrical properties. In fact, the film B-10-150 has the lowest resistance (49.5 Ω, measured by hall effect analysis) than the others. The carrier density and carrier mobility measured for the B-10-150 are 5.6×10^{16} cm^{-3} and 4.7 $cm^2/(V\ s)$, respectively. The results showed a high mobility with low carrier concentration, which is beneficial for a window layer where free carrier absorption shall be minimized. Another impact of high oxygen doping is the reduced voltage with increasing doping level. It is likely that the defects at the surface are recombination sites that shunt the device. Our results implied that there seems to be an optimal doping level that yields the most suitable properties for NiOx as blocking layer for this device. Once the film is overdoped, the defects introduced by the excess oxygen will result in highly disorder materials with high resistivity and deteriorate the photovoltaic performances. Another possibility is the surface states (Ni^{3+} as confirmed by the XPS) incorporated with high oxygen doping will act as trap states that facilitate interfacial charge recombination and reduce our current and voltage output. Figure 4d illustrates the incident photon-to-electron conversion efficiency (IPCE) response of these devices. From Figure 4d, it can be apparently observed that devices B-5-150, B-10-150, and B-15-150 showed higher IPCE responses below 500 nm than device A-0-150. The high-energy photons are absorbed in the perovskite at the light incident side close to the NiOx surface. The doping could probably increase conductivity and resulted in better charge collection. This interesting feature is still under investigation. On the other hand, as oxygen flow ratio increased to 15%, the photocurrent density of device B-15-150 dramatically decreased to 14.4 mA cm^{-2}. As can be seen in Figure 4d, the IPCE values of device B-15-150 in the range between 500 and 770 nm are relatively lower by 20% than the others. According to its comparatively high resistance (0.27 kΩ, measured by hall effect analysis), we expect the highly doping of oxygen introduced interstitial oxygen defects and Ni vacancies, which lead to inferior crystallinity (as shown in XRD and XPS) and stronger scattering for carrier transport. Therefore, excess oxygen flow ratio during sputtering end up with detrimental effects for device performance. Device using NiOx film deposited under oxygen flow ratio of 10% (B-10-150) delivered the best conversion efficiency of 11.6% with open-circuit voltage of 0.96 V, short-circuit current density of 19.8 mA cm^{-2}, and fill factor of 0.61. It is noticed that the AM1.5 G and IPCE integrated current value are considerably lower (10–20%) compared with the short circuit current measured from the IV protocol. The IPCE and AM1.5G integrated values are presented in Table 4. The value could differ from the short circuit current due to the mismatch between light source and AM1.5G, or nonlinearity of photovoltaic performance against light intensity. Normally, a 10% difference is considered as an acceptable value. We have to point out that the IV characterizations are measured inside the glovebox right after the device fabrication. However, the IPCEs are measured under atmosphere without encapsulation so that the oxidation of PCBM or degradation from perovskite can occur. We have tested the evolution of the IPCE as the exposure time in atmosphere (see Figure S4 in the Supporting Information). It is obvious that the IPCE suffered degradation within the first 30 min. These could be the reason that our IPCE values are lowered than the short circuit current obtained from IV characteristics.

Recently, many highly efficient perovskite photovoltaic devices are constructed as thin film (or planar heterojucntion) solar cells where no nanocrystallines are required.[5,6,9] The low-temperature sputtering process reported in this article has the advantage to compatibly work with the flexible devices using planar perovskite-based hetrojunction architecture without mesoscopic layer. This provides a robust inorganic alternative to the most commonly used low-temperature solution-processed organic hole extraction layer for perovskite-based solar cells.

In this report, we employed low-temperature sputtered NiOx thin film as hole extraction and electron blocking layer for mesoscopic NiO/$CH_3NH_3PbI_3$ heterojunction solar cells. We found the film thickness of NiOx compact layer plays an important role in device performance. Moreover, with adequate oxygen doping, the photovoltaic performance of device could be further enhanced. We have realized the first report that investigates the use of sputtered NiOx thin film on the photovoltaic performance of perovskite-based solar cells with the effects on film thickness and oxygen flow ratios. The mesoscopic NiO/$CH_3NH_3PbI_3$ photovoltaic devices using this method remarkably improved in both photocurrent and overall efficiency compared with our previous work using solution based NiOx thin film. The best cell made with adequate oxygen

flow doping of 10%, achieved device efficiency of 11.6% with J_{SC} as high as 19.8 mA cm^{-2}.

■ ASSOCIATED CONTENT

Supporting Information

Experimental procedures, Mott−Schottky plot, photo of NOx sputtered substrates, absorbance of perovskite coated on mesoscopic NiO film, IPCE evolution in atmosphere. This material is available free of charge via the Internet at http://pubs.acs.org/

■ AUTHOR INFORMATION

Corresponding Author

*E-mail: petercyc@mail.ncku.edu.tw.

Notes

The authors declare no competing financial interest.

■ ACKNOWLEDGMENTS

P.C. appreciates the research funding from the Ministry of Science and Technology (MOST) of Taiwan (NSC102-2113-M-006-010) and the financial support from the Top-Notch Project under the Headquarter of University Advancement at National Cheng Kung University, which is sponsored by the Ministry of Education, Taiwan, ROC. T.F.G. thanks the MOST of Taiwan (NSC102-2682-M-006-001-MY3) for financially supporting this research.

■ REFERENCES

(1) Wang, K.-C.; Jeng, J.-Y.; Shen, P.-S.; Chang, Y.-C.; Diau, E. W.-G.; Tsai, C.-H.; Chao, T.-Y.; Hsu, H.-C.; Lin, P.-Y.; Chen, P.; Guo, T.-F.; Wen, T.-C. p-Type Mesoscopic Nickel Oxide/Organometallic Perovskite Heterojunction Solar Cells. *Sci. Rep.* **2014**, *4*, 4756.

(2) Kim, H.-S.; Lee, C.-R.; Im, J.-H.; Lee, K.-B.; Moehl, T.; Marchioro, A.; Moon, S.-J.; Humphry-Baker, R.; Yum, J.-H.; Moser, J. E.; Grätzel, M.; Park, N.-G. Lead Iodide Perovskite Sensitized All-Solid-State Submicron Thin Film Mesoscopic Solar Cell with Efficiency Exceeding 9%. *Sci. Rep.* **2012**, *2*, 591.

(3) Lee, M. M.; Teuscher, J.; Miyasaka, T.; Murakami, T. N.; Snaith, H. J. Efficient Hybrid Solar Cells Based on Meso-Superstructured Organometal Halide Perovskites. *Science* **2012**, *338*, 643−647.

(4) Burschka, J.; Pellet, N.; Moon, S.-J.; Humphry-Baker, R.; Gao, P.; Nazeeruddin, M. K.; Grätzel, M. Sequential Deposition as a Route to High-Performance Perovskite-Sensitized Solar Cells. *Nature* **2013**, *499*, 316−319.

(5) Liu, M.; Johnston, M. B.; Snaith, H. J. Efficient Planar Heterojunction Perovskite Solar Cells by Vapour Deposition. *Nature* **2013**, *501*, 395−398.

(6) Liu, D.; Kelly, T. L. Perovskite Solar Cells with a Planar Heterojunction Structure Prepared Using Room-Temperature Solution Processing Techniques. *Nat. Photonics* **2014**, *8*, 133−138.

(7) Kojima, A.; Teshima, K.; Shirai, Y.; Miyasaka, T. Organometal Halide Perovskites as Visible-Light Sensitizers for Photovoltaic Cells. *J. Am. Chem. Soc.* **2009**, *131*, 6050−6051.

(8) Chen, Q.; Zhou, H.; Hong, Z.; Luo, S.; Duan, H.-S.; Wang, H.-H.; Liu, Y.; Li, G.; Yang, Y. Planar Heterojunction Perovskite Solar Cells via Vapor-Assisted Solution Process. *J. Am. Chem. Soc.* **2014**, *136*, 622−625.

(9) Docampo, P.; Ball, J. M.; Darwich, M.; Eperon, G. E.; Snaith, H. J. Efficient Organometal Trihalide Perovskite Planar-Heterojunction Solar Cells on Flexible Polymer Substrates. *Nat. Commun.* **2013**, *4*, 2761.

(10) Jeng, J.-Y.; Chiang, Y.-F.; Lee, M.-H.; Peng, S.-R.; Guo, T.-F.; Chen, P.; Wen, T.-C. $CH_3NH_3PbI_3$ Perovskite/Fullerene Planar-Heterojunction Hybrid Solar Cells. *Adv. Mater.* **2013**, *25*, 3727−3732.

(11) You, J.; Hong, Z.; Yang, Y.; Chen, Q.; Cai, M.; Song, T.-B.; Chen, C.-C.; Lu, S.; Liu, Y.; Zhou, H.; Yang, Y. Low-Temperature Solution-Processed Perovskite Solar Cells with High Efficiency and Flexibility. *ACS Nano* **2014**, *8*, 1674−1680.

(12) Jørgensen, M.; Norrman, K.; Krebs, F. C. Stability/Degradation of Polymer Solar Cells. *Sol. Energy Mater. Sol. Cells* **2008**, *92*, 686−714.

(13) Sun, Y.; Takacs, C. J.; Cowan, S. R.; Seo, J. H.; Gong, X.; Roy, A.; Heeger, A. J. Efficient, Air-Stable Bulk Heterojunction Polymer Solar Cells Using MoOx as the Anode Interfacial Layer. *Adv. Mater.* **2011**, *23*, 2226−2230.

(14) Jeng, J.-Y.; Chen, K.-C.; Chiang, T.-Y.; Lin, P.-Y.; Tsai, T.-D.; Chang, Y.-C.; Guo, T.-F.; Chen, P.; Wen, T.-C.; Hsu, Y.-J. Nickel Oxide Electrode Interlayer in $CH_3NH_3PbI_3$ Perovskite/PCBM Planar-Heterojunction Hybrid Solar Cells. *Adv. Mater.* **2014**, *26*, 4107−4113.

(15) Subbiah, A. S.; Halder, A.; Ghosh, S.; Mahuli, N.; Hodes, G.; Sarkar, S. K. Inorganic Hole Conducting Layers for Perovskite-Based Solar Cells. *J. Phys. Chem. Lett.* **2014**, *5*, 1748−1753.

(16) Tian, H.; Xu, B.; Chen, H.; Johansson, E. M. J.; Boschloo, G. Solid-State Perovskite-Sensitized p-Type Mesoporous Nickel Oxide Solar Cells. *ChemSusChem* **2014**, doi: 10.1002/cssc.201402032, accessed 24 APR 2014.

(17) Christians, J. A.; Fung, R. C. M.; Kamat, P. V. An Inorganic Hole Conductor for Organo-Lead Halide Perovskite Solar Cells. Improved Hole Conductivity with Copper Iodide. *J. Am. Chem. Soc.* **2014**, *136*, 758−764.

(18) Ito, S.; Tanaka, S.; Vahlman, H.; Nishino, H.; Manabe, K.; Lund, P. Carbon-Double-Bond-Free Printed Solar Cells from TiO_2/$CH_3NH_3PbI_3$/CuSCN/Au: Structural Control and Photoaging Effects. *ChemPhysChem* **2014**, *15*, 1194−1200.

(19) Qin, P.; Tanaka, S.; Ito, S.; Tetreault, N.; Manabe, K.; Nishino, H.; Nazeeruddin, M. K.; Grätzel, M. Inorganic Hole Conductor-Based Lead Halide Perovskite Solar Cells with 12.4% Conversion Efficiency. *Nat. Commun.* **2014**, *5*, 3834.

(20) Irwin, M. D.; Buchholz, D. B.; Hains, A. W.; Chang, R. P. H.; Marks, T. J. p-Type Semiconducting Nickel Oxide as an Efficiency-Enhancing Anode Interfacial Layer in Polymer Bulk-Heterojunction Solar Cells. *Proc. Natl. Acad. Sci. U. S. A.* **2008**, *105*, 2783−2787.

(21) Hancox, I.; Rochford, L. A.; Clare, D.; Sullivan, P.; Jones, T. S. Utilizing n-Type Vanadium Oxide Films as Hole-Extracting Layers for Small Molecule Organic Photovoltaics. *Appl. Phys. Lett.* **2011**, *99*, 013304.

(22) Lee, Y.-J.; Yi, J.; Gao, G. F.; Koerner, H.; Park, K.; Wang, J.; Luo, K.; Vaia, R. A.; Hsu, J. W. P. Low-Temperature Solution-Processed Molybdenum Oxide Nanoparticle Hole Transport Layers for Organic Photovoltaic Devices. *Adv. Energy Mater.* **2012**, *2*, 1193−1197.

(23) Tian, H.; Oscarsson, J.; Gabrielsson, E.; Eriksson, S. K.; Lindblad, R.; Xu, B.; Hao, Y.; Boschloo, G.; Johansson, E. M. J.; Gardner, J. M.; Hagfeldt, A.; Rensmo, H.; Sun, L. Enhancement of p-Type Dye-Sensitized Solar Cell Performance by Supramolecular Assembly of Electron Donor and Acceptor. *Sci. Rep.* **2014**, *4*, 4282.

(24) Powar, S.; Daeneke, T.; Ma, M. T.; Fu, D.; Duffy, N. W.; Götz, G.; Weidelener, M.; Mishra, A.; Bäuerle, P.; Spiccia, L.; Bach, U. Highly Efficient p-Type Dye-Sensitized Solar Cells based on Tris(1,2-diaminoethane)Cobalt(II)/(III) Electrolytes. *Angew. Chem., Int. Ed.* **2013**, *52*, 602−605.

(25) Nandy, S.; Saha, B.; Mitra, M. K.; Chattopadhyay, K. K. Effect of Oxygen Partial Pressure on the Electrical and Optical Properties of Highly (200) Oriented p-Type Ni_{1-x} O Films by DC Sputtering. *J. Mater. Sci.* **2007**, *42*, 5766−5772.

(26) Guziewicz, M.; Grochowski, J.; Borysiewicz, M.; Kaminska, E.; Domagala, J. Z.; Rzodkiewicz, W.; Witkowski, B. S.; Golaszewska, K.; Kruszka, R.; Ekielski, M.; Piotrowska, A. Electrical and Optical Properties of NiO Films Deposited by Magnetron Sputtering. *Opt. Appl.* **2011**, *41*, 431−440.

(27) Christian, J.; Gilbreath, W. Defect Structure of NiO and Rates and Mechanisms of Formation from Atomic Oxygen and Nickel. *Oxid. Met.* **1975**, *9*, 1−25.

(28) Mrowec, S.; Grzesik, Z. Oxidation of Nickel and Transport Properties of Nickel Oxide. *J. Phys. Chem. Solids* **2004**, *65*, 1651−1657.

(29) Peng, B.; Jungmann, G.; Jäger, C.; Haarer, D.; Schmidt, H.-W.; Thelakkat, M. Systematic Investigation of the Role of Compact TiO_2

Layer in Solid State Dye-Sensitized TiO_2 Solar Cells. *Coord. Chem. Rev.* **2004**, *248*, 1479−1489.
(30) Reddy, Y. A. K.; Reddy, A. M.; Reddy, A. S.; Reddy, P. S. Preparation and Characterization of NiO Thin Films by DC Reactive Magnetron Sputtering. *J. Nano-Electron. Phys.* **2012**, *4*, 04002.